

PHASE DIAGRAMS AS TOOLS FOR ADVANCED MATERIALS DESIGN: APPLICATIONS TO NON-FERROUS ALLOYS

Ikuo Ohnuma¹
Kiyohito Ishida²

Abstract

It is recognized that phase diagrams and a thermodynamic database constructed by the CALPHAD (Calculation of Phase Diagrams) approach play an important role in alloy design and materials development. In this paper, recent progress on the thermodynamic database for micro-solders and Cu-base alloys, which is useful for the development of Pb-free solders and predictions of interfacial phenomena between solders and the Cu substrate in electronic packaging technology, is presented. In addition, typical examples of the application of phase diagrams are presented to facilitate the development of shape memory alloys, Co-Cr base magnetic recording media, ferromagnetic Heusler alloys and Co base superalloys.

Keywords: CALPHAD; Pb-free solders; Co-Cr magnetic recording media; Co based superalloys; Alloy design; Phase diagrams

DIAGRAMAS DE FASES COMO FERRAMENTA NO PROJETO DE MATERIAIS AVANÇADOS- APLICACOES A LIGAS NÃO-FERROSAS

Resumo

Já é bem aceito que diagramas de fases e um banco de dados termodinamicos construídos através do enfoque CALPHAD (Calculation of Phase Diagrams) tem um papel importante no projeto de ligas e no desenvolvimento de materiais. Neste artigo, são apresentados os recentes progressos nos bancos de dados para micro-soldas e ligas a base de cobre, que são úteis para o desenvolvimento de soldas isentas de Pb e para as previsões dos fenômenos interfaciais entre estas soldas e os substratos de Cu na tecnologia de montagem de componentes eletrônicos. Adicionalmente, exemplos típicos da aplicação de diagramas de fases no auxilio do desenvolvimento de ligas de memória de forma, ligas Co-Cr para mídia de gravação magnética de dados, ligas ferromagnéticas do tipo Heusler e superligas a base de Co são apresentados e discutidos.

Palavras-chave: CALPHAD; Ligas para soldagem isentas de Pb; Ligas para mídia de gravação magnética Co-Cr; Superligas a base de Co; Projeto de ligas; Diagramas de fases.

1 INTRODUCTION

Since the pioneering work in the computer calculation of phase diagrams by Kaufman and Bernstein [1] in 1970, the CALPHAD (computer coupling of phase diagrams and thermochemistry) method [2,3] has been established due to progress in computer software such as Thermo-Calc [4], Fact-Sage [5,6], Pandat [7], etc., which are widely used for materials design. Thermodynamic databases are now available for several alloy systems, such as Fe, Ni, Ti, Al, Mg-based alloys, ceramic systems and alloy semiconductors, as shown in Table I.

These thermodynamic databases have been developed based on experimental data of thermodynamic properties and phase equilibria in the literature, as shown in Figure 1.

Recently, calculated results obtained by first principle calculation have also been applied to thermodynamic assessment in the same way with the experimental data. Once the thermodynamic databases have been constructed, many types of properties indispensable for alloy design, computer simulation, etc., can be predicted by the above-mentioned software for calculation.

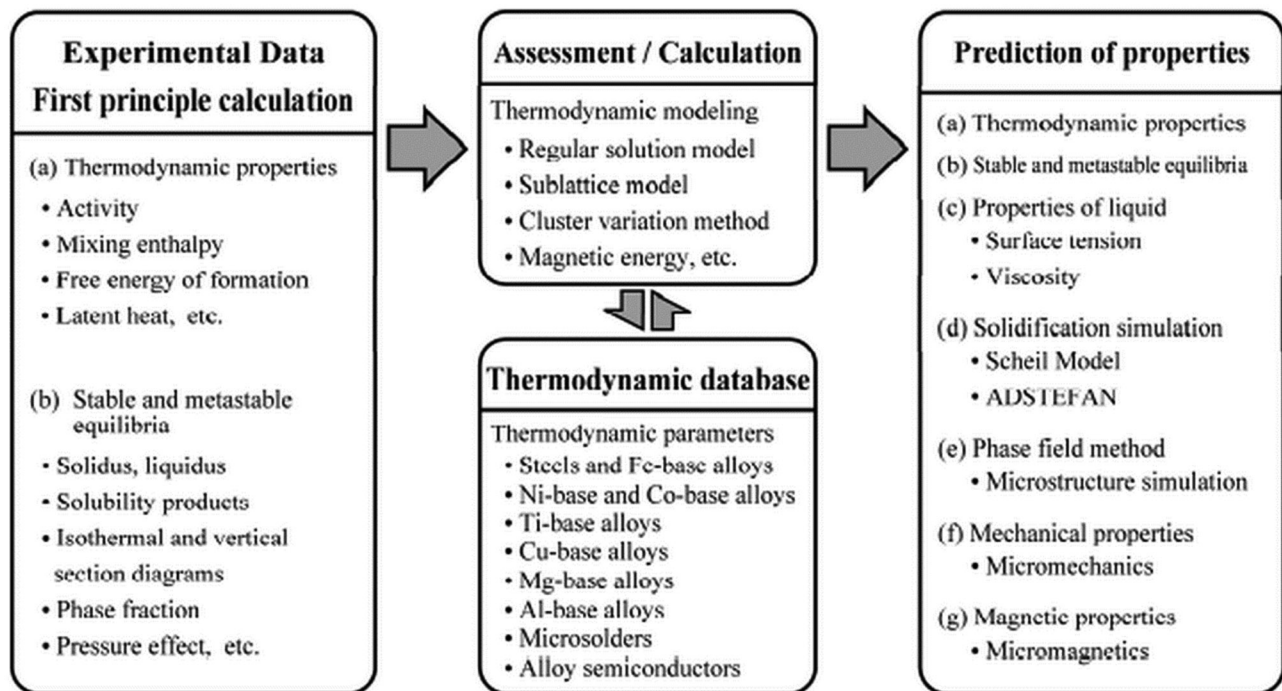
¹Computational Materials Science Unit, National Institute for Materials Science – NIMS, Tsukuba, Japan.

²Department of Materials Science, Tohoku University, Sendai, Japan. E-mail: ishida@material.tohoku.ac.jp



Table I. Thermodynamic databases for various alloy systems

Alloy systems	Elements	Phases
Iron base alloys		
Low alloy steels	Fe-C-N-Si-Mn-Cr-Mo-Ni-Co-Al-Nb-V-Ti-W	L, α , γ , carbides, nitrides
Microalloyed steels	Fe-C-N-S-Mn-Si-Al-Cr-Ti-Nb-V	L, α , γ , carbides, nitrides, sulfides
Tool steels	Fe-C-Cr-V-W-Mo-Co	L, α , γ , carbides
Stainless steels	Fe-C-N-Si-Cr-Ni-Mn-Mo-Al	L, α , γ , carbides, nitrides
Steels with low density	Fe-C-Mn-Al-Cr-Si	L, α , γ , carbides
Sulfides	Fe-C-S-Cr-Ni-Mn-Ti	L, α , γ , sulfides, carbides
Ni base alloys	Ni-Al-Ti-Cr-Mo-Co-Ta-Nb-Zr-W-Hf-B-C	L, γ , γ' , β , TCP(σ , μ , Laves), borides, carbides
Co base alloys	Co-Al-B-C-Cr-Cu-Fe-Mn-Mo-Nb-Ni-Pt-Re-Si-Ta-Ti-W	L, α , ϵ , intermetallic compounds (IMCs)
Ti base alloys	Ti-Al-V-Mo-Cr-Si-Fe-Nb-Sn-Ta-Zr-B-C-N-O	L, α , β , IMCs, borides, carbides, oxides, nitrides
Al base alloys	Al-Cr-Cu-Fe-Mg-Mn-Ni-Si-Ti-V-Zn-Zr	L, α , IMCs
Mg base alloys	Mg-Al-Ca-Ce-Gd-Li-Mn-Nd-Sc-Si-Sr-Y-Zn-Zr	L, α , β , γ , IMCs
Cu base alloys	Cu-B-C-Cr-Fe-Ni-P-Si-Sn-Ti-Zn	L, α , β , γ , IMCs
Alloy semiconductor	Al-Ga-In-P-As-Sb	L, compounds
Microsolders	Pb-Sn-Ag-Cu-Bi-Sb-Zn-In-(Al)-(Au)-(Ni)	L, α , β , γ , δ , IMCs

**Figure 1.** Development and application of thermodynamic databases.

Recently, the present authors have developed thermodynamic databases for micro-soldering materials [8-10] and Cu-base alloys [11,12] within the framework of the CALPHAD method. These databases are useful for the alloy design of Pb-free solders and Cu-base substrate materials, as well as for understanding the interfacial reaction between them. In addition, we are also constructing a thermodynamic database for Co-base alloys, which is practically important for heat-resistant and corrosion-resistant alloys, magnetic alloys, bio-materials, etc. In this paper, focusing on micro-solders, Cu-base alloys, Co-Cr magnetic recording media, Ni-Mn-In ferromagnetic shape memory alloys and Co-base superalloys,

the role of phase diagrams and thermodynamic databases in materials design is presented.

2 ELECTRONIC MATERIALS

2.1 Design of Micro-soldering Materials

During the past several decades, Pb-free solders to replace conventional Pb-Sn alloys have been designed and developed to satisfy the requirements arising from environmental and health issues concerning the toxicity

of Pb [13]. For the development of suitable alternatives to Pb-Sn solders, the melting temperature is one of the most important properties to be optimized. A thermodynamic database of micro-soldering materials named ADAMIS (Alloy Database for Micro-Solders) listed in Table 1 has been developed [8-10], by which phase equilibria can be calculated in the whole composition range for the elements Ag, Bi, In, Cu, Sn, Sb, Zn and Pb and in a limited composition range for Al and Au. Figure 2 shows the liquidus surface projection of six Sn-base ternary systems calculated using the ADAMIS database [14], in which the isothermal liquidus lines and reaction types are indicated. Melting temperatures of Sn-base ternary alloys can be predicted at a glance using these calculated diagrams.

The solidification process of solders is also an important factor for the alloy design of Pb-free solders. Although the Scheil model assumes that local equilibrium occurs at the liquid/solid interface and that diffusion is absent in the solidified phases, such calculations can still provide useful information for the prediction of reality. Solidification simulation of a promising candidate as an alternative to Pb-Sn solders, Sn-2.0Ag-0.5Cu-7.5Bi (mass%) alloy, has been carried out. Figure 3 shows the variation of the calculated mass fraction of the solid phases with the temperature of this alloy under equilibrium and Scheil model solidification conditions.

In both cases, the solidification starts with the primary crystals of η -Cu₆Sn₅, and the liquid phase disappears at 177.9°C under the equilibrium solidification condition. According to the Scheil model, however, Bi is concentrated in the liquid phase during solidification, which causes an extensive fall of the terminating temperature of solidification (139.9°C), corresponding to the eutectic reaction of the Sn-Bi binary system. Many other properties related to phase diagrams can be calculated and can be used for the development of Pb-free solders not only for conventional temperature ranges around 200°C but also for high temperature applications above 300°C.

2.2 Egg-type Microstructures

Recently, we have shown that an egg-like core/shell microstructure can be obtained in powder particles prepared by conventional gas atomization [15], in which the minor liquid phase always forms the core of the egg. Since this finding, extensive studies have been carried out on the mechanism [16-18] of the formation of the egg-type microstructure, the role of interfacial energy [19] and bulk ingots with a core-type microstructure [20]. Figure 4 shows a schematic illustration of the relation between the microstructure of powder particles and a liquid phase miscibility gap in a phase diagram [21].

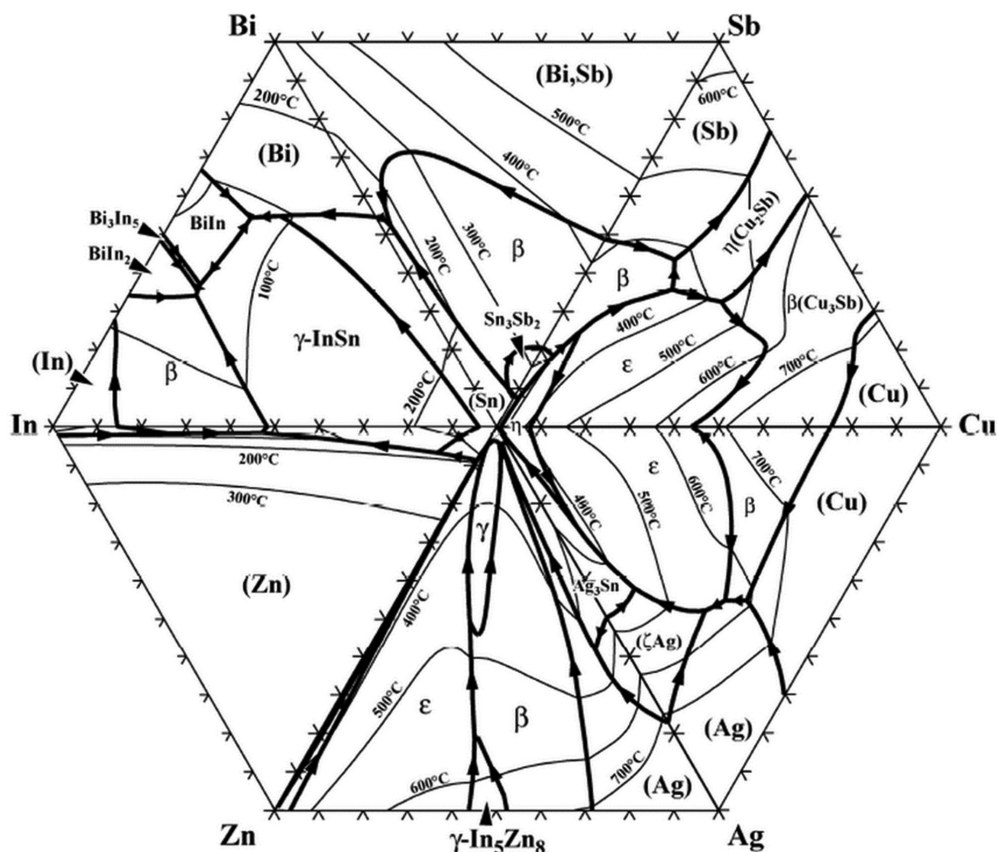


Figure 2. Liquidus surface projection diagrams in the Sn-base ternary systems.

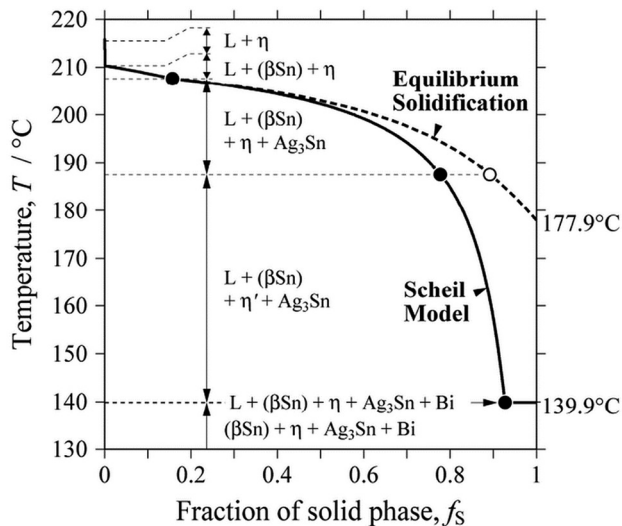


Figure 3. Solidification simulation of Sn-2Ag-0.5Cu-7.5Bi alloy.

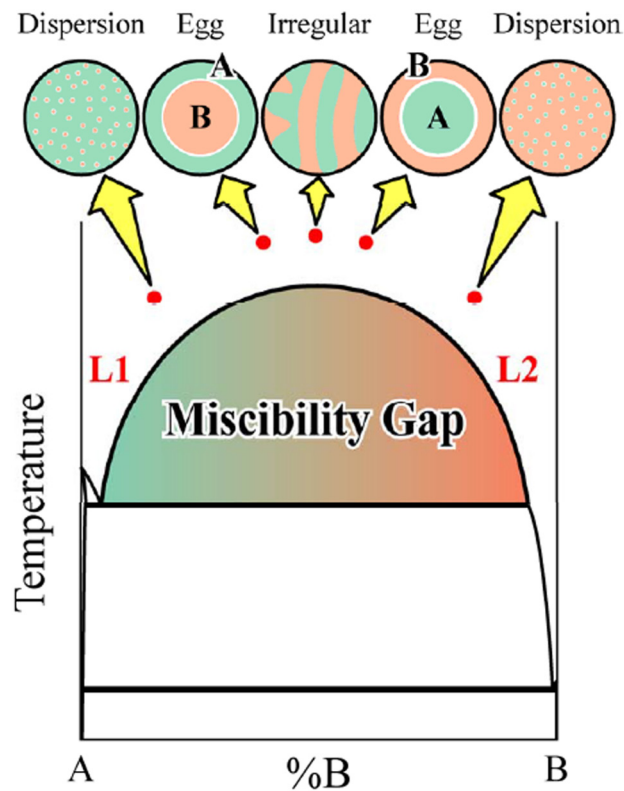


Figure 4. Schematic illustration of microstructural evolution of powder particles related to the phase diagram with liquid phase miscibility gap.

An egg-type core/shell structure is formed when the chemical composition of an alloy is located in the middle portion of the miscibility gap, while the *in situ* composite which shows that a fine second phase dispersed in the matrix is formed just inside both ends of the miscibility gap. Therefore, thermodynamic calculation of the liquid miscibility gap plays a key role in the study of the microstructural evolution of powder.

Bi-based alloys are candidates for high-temperature Pb-free solders. Figure 5d shows a calculated phase diagram of the Bi-Cu-Sn ternary system at 650°C, in which a metastable liquid phase miscibility gap in the Bi-Cu binary system is stabilized by the addition of Sn.

Thus, the formation of the egg-type microstructure can be expected in this ternary system. Since the details of Bi-based solder properties such as phase relation, microstructure, interfacial reaction, reliability, etc., have already been reported [21-23], only typical microstructures of an egg-type core/shell and *in situ* composite powder particles are shown in Figures 5a and 5c, respectively. The shell of egg-type particles and the matrix of the *in situ* composite consist of a Bi-rich phase which plays the role of high-temperature solder. On the other hand, a Cu-Sn intermetallic compound forms the core and dispersion particles, which are expected to improve the mechanical properties. The melting temperatures have been found to be about 270°C and 730°C, which correspond to those of Bi-rich phase and Cu₃Sn-compound [21].

On the other hand, three kinds of Ag-based powders with high electrical conductivity, i.e., Ag-Cu-Ni, Ag-Cu-Co and Ag-Cu-Fe alloys, were prepared making use of the egg-type microstructure caused by immiscible liquid [24]. In these ternary systems, the morphology of the powder obtained by the gas-atomizing method is schematically summarized in Figure 6.

The *in situ* composite and egg-type micro-powders can be produced from immiscible alloys whose chemical composition is located near both ends and around the middle of the miscibility gap, respectively. In between these two composition regions shown by the shaded areas in Figure 6, mixed powder of *in situ* composite and egg-type microstructures can be obtained.

2.3 High-strength and High-conductive Cu-Ni-Al Based Alloys

In the field of materials science, combinatorial techniques, for instance making use of a diffusion couple (DC) or triple (DT) samples, has been recognized as a powerful and effective method for the determination of phase diagrams, including not only equilibrium compositions but also transition boundaries of martensite/austenite, ferro-/para-magnetic, order/disorder phases, etc., simultaneously in a wide range of chemical composition [25]. Here we would like to show how the combinatorial technique was applied to develop high-strength and high-conductive Cu-Ni-Al based alloys. Figure 7 shows the isothermal section phase diagram of the Cu-Ni-Al ternary system at 500°C calculated from the thermodynamic database, where the two-phase region of fcc (Cu) and L₁ (Ni₃Al) phases are predicted.

This two-phase region is expected to have high strength and high electrical conductivity strengthened by Ni₃Al precipitation. To find the optimum compositions, the combinatorial method was used.

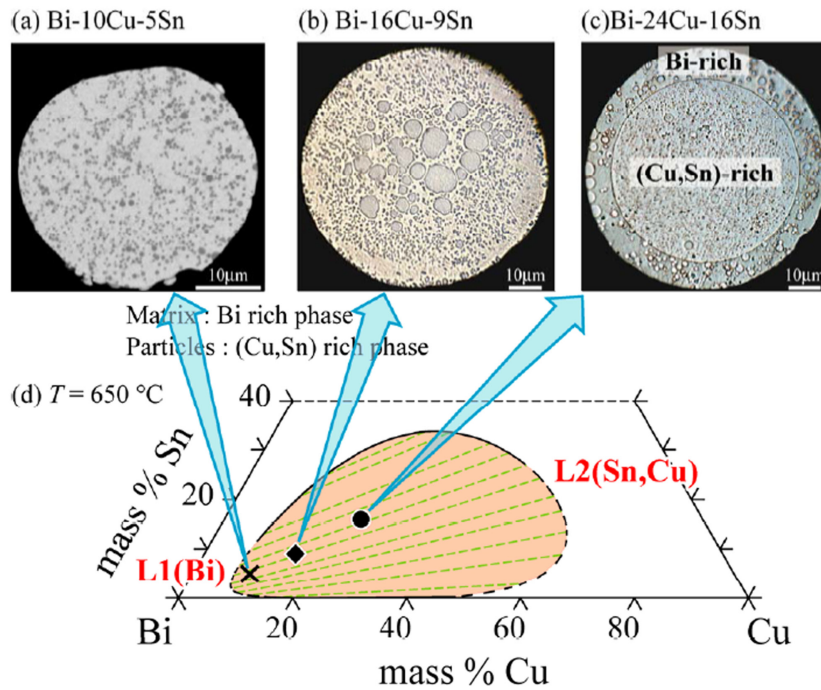


Figure 5. Stable and metastable liquid phase miscibility gap (LPMG) at 650°C in the Bi-Cu-Sn ternary system; (d). Microstructures of gas-atomized particles of (a) edge of the LPMG (Bi-10Cu-5Sn); (c) middle of the LPMG (Bi-24Cu-16Sn) and (b) intermediate (Bi-16Cu-9Sn).

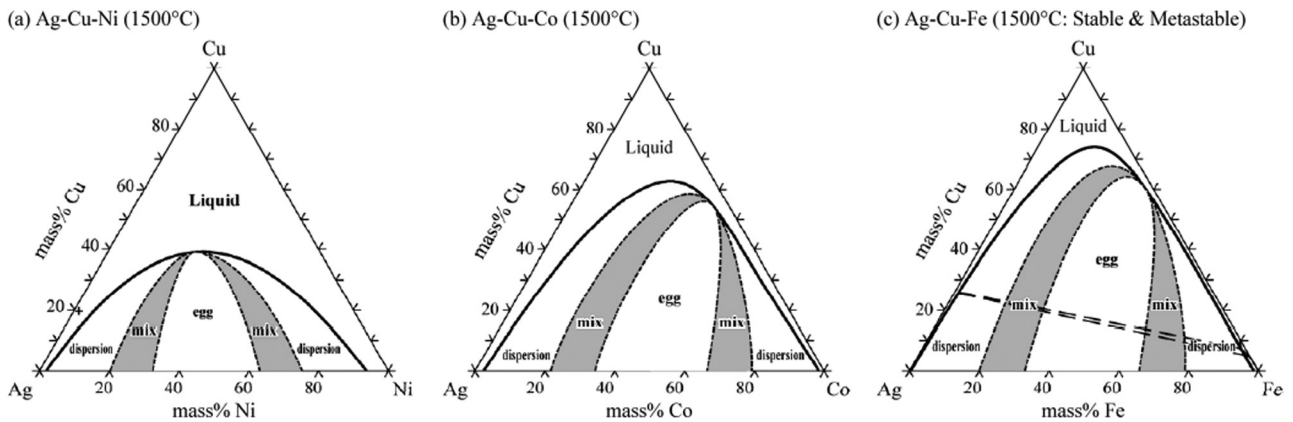


Figure 6. Microstructural evolution related to liquid miscibility gap in (a) Ag-Cu-Ni; (b) Ag-Cu-Co and (c) Ag-Cu-Fe systems.

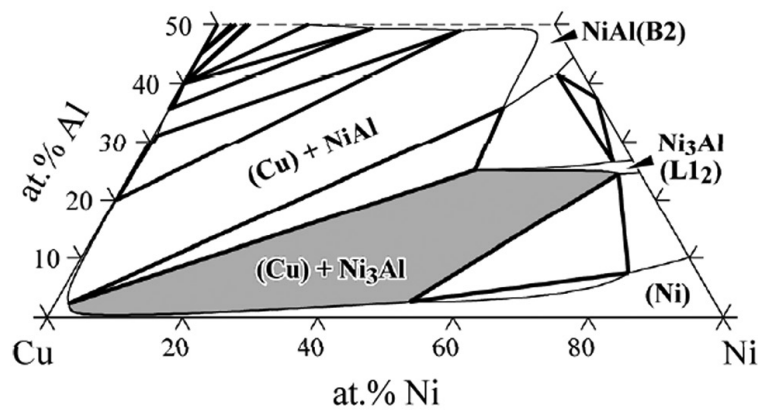


Figure 7. Calculated phase diagram at 500°C in the Cu-Ni-Al ternary system. Shaded area represents a miscibility gap between the fcc (Cu) and L₁₂ Ni₃Al phases.

Ingots of pure Cu, Cu-30Ni and Cu-20Al (mass%) were prepared by induction melting. Each ingot was cut into small cubic pieces, the surfaces of which were mechanically polished to remove contaminated layers. Cubic samples of Cu and Cu-30Ni were first diffusion bonded at 900°C for 1 hour. The Cu/Cu-30Ni diffusion couples and Cu-Al alloys were diffusion bonded as the Cu/Cu-30Ni interface was aligned perpendicular to the bonded surface of the Cu-Al samples. The prepared DT samples were heat-treated at 1000°C for 60 days to obtain the solid solution fcc-(Cu) phase, in which considerable amounts of Ni and Al were solved to form a wide range of chemical compositions in one DT sample. After that, the solution-treated DT samples were aged at 500°C for 6 to 18 hours to obtain a precipitated microstructures, which can be predicted from the calculated phase diagram shown in Figure 7. Chemical compositions of the solution-treated DT samples were determined by an Election Probe Micro Analyser (EPMA) (JEOL, JXA-8100). Vickers hardness and conductivity were measured by a micro Vickers hardness tester (Akashi, MVK-H1) and an electrical resistance tester for tiny areas equipped with a 0.1 mm-interstices four-point probe, respectively. Precipitated microstructures of aged DT samples were examined by a TEM (JEOL, JEM-2000EXII).

Figure 8 shows a dark field image taken from a (100) $L1_2$ super-lattice reflection of Cu-12.3Ni-1Al-0.3Si (mass%) alloy aged at 500°C for 12 h, the chemical composition of which was optimized based on results of combinatorial experiments.

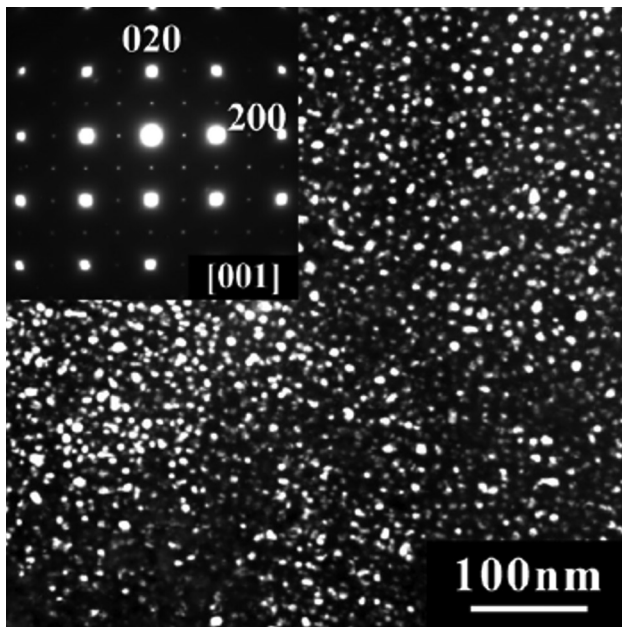


Figure 8. TEM dark-field image taken from (100) $L1_2$ super-lattice reflection and selected area diffraction pattern with the incident beam direction of [001]. $L1_2$ Ni_3Al particles are finely dispersed in fcc (Cu) matrix in Cu-12.3Ni-1Al-0.5Si (mass%) alloy solution-treated at 900°C for 10 min, 30% cold-rolled and aged at 500°C for 12 h.

Fine particles of the $L1_2$ - Ni_3Al phase were dispersed presumably due to the spinodal decomposition, which results in a considerable increase of both hardness and electrical conductivity. The relationship between the tensile strength and electrical conductivity is summarized in Figure 9. Optimized Cu-Ni-Al-Si alloys, which show especially high-strength properties, can be substituted for conventional Cu-Be alloys. This alloy system has been commercialized as suspension wire for optical pickup in DVD drives.

3 SHAPE MEMORY ALLOYS

3.1 Cu-Mn-Al Shape Memory Alloys

Cu-based shape memory alloys (SMAs) such as Cu-Al- and Cu-Zn-based alloys are commercially attractive for practical applications of the shape memory effect (SME) and pseudo elasticity (PE) because of their low cost and their advantages with regard to electrical and thermal conductivities. However, the polycrystalline Cu-based SMAs are generally brittle and tend to cause intergranular fractures due to their high degree of order in the parent β phase with $B2$, $D0_3$ or $L2_1$ structure and the extremely high elastic anisotropy ratio in the β phase [26]. Kainuma et al. [27] have reported that excellent ductility can be obtained by controlling the degree of order in the β phase of the Cu-Al-Mn SMAs. Figures 10a and 10b show the isothermal section phase diagram at 850°C [28] and vertical ones of Cu-Al-10at.%Mn alloys [29], respectively. This system is well-known for the

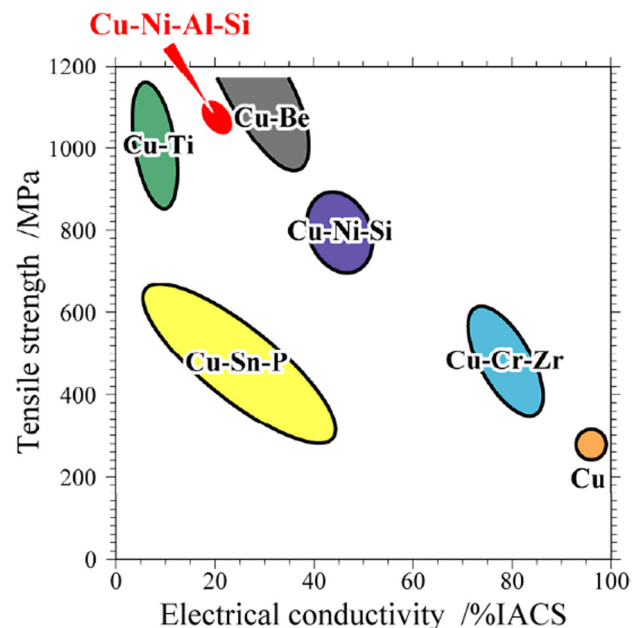


Figure 9. Relationship between tensile strength and electrical conductivity of developed Cu-Ni-Al-Si alloy in comparison with conventional Cu-base alloys.

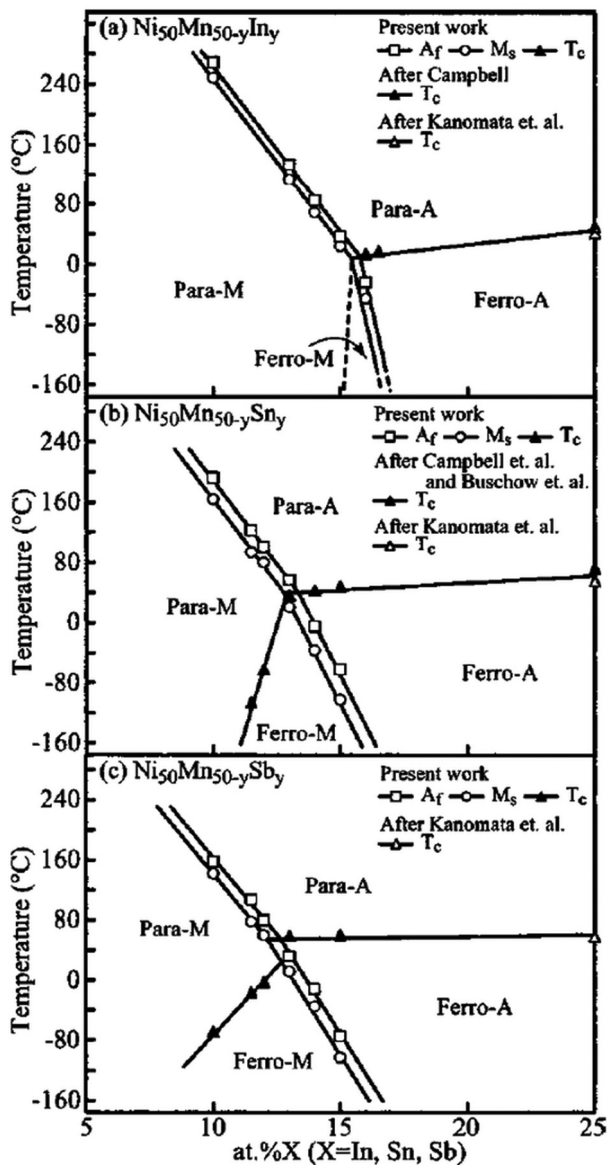


Figure 12. Martensitic and magnetic transition temperatures of the (a) $\text{Ni}_{50}\text{Mn}_{50-y}\text{In}_y$; (b) $\text{Ni}_{50}\text{Mn}_{50-y}\text{Sn}_y$ and (c) $\text{Ni}_{50}\text{Mn}_{50-y}\text{Sb}_y$ alloys, where Para and Ferro mean paramagnetic and ferromagnetic, respectively, and A and M indicate the austenite and martensite, respectively. See Sutou et al. [38] for additional information.

be below -200°C Figure 13 shows the thermo-magnetization curves for the 13.4 In alloy at magnetic field strengths of $H = 0.5, 20$ and 70 kOe [39].

During the initial heating in a magnetic field of $H = 0.5$ kOe, the thermo-magnetization curve drastically decreased between 375 K and 390 K owing to the transformation from ferromagnetic (or ferrimagnetic) to paramagnetic in the parent phase, where the Curie temperature T_c was calculated to be $T_c = 382$ K. The magnetism of the parent phase below T_c is considered to be ferromagnetic rather than ferrimagnetic because the temperature dependence of the reciprocal susceptibility in the paramagnetic state follows the

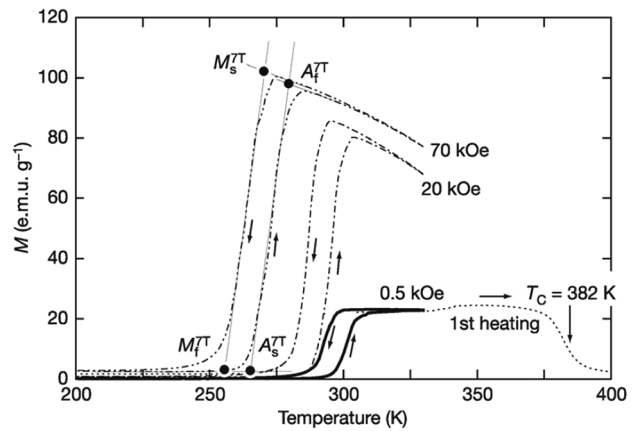


Figure 13. Thermo-magnetization curves of the $\text{Ni}_{45}\text{Co}_5\text{Mn}_{36.6}\text{In}_{13.4}$ alloy measured in several magnetic fields.

normal Curie-Weiss law. After heating to 473 K followed by furnace cooling, the magnetization was cyclically measured at temperatures between 200 K and 330 K in magnetic fields of $H = 0.5, 20$ and 70 kOe. The magnetization curve of 0.5 kOe declined suddenly at about 292 K as a result of the martensitic transformation and entered a steady region with a very low magnetization on cooling. Furthermore, the magnetization drastically increased at about 300 K as a result of the reverse transformation with a small thermal hysteresis of less than 10 K on heating. Figure 14 shows the magnetization curves at several temperatures. While the curves at 200 K and 320 K exhibit typical non-magnetic and ferromagnetic M-H behaviors, respectively, the curves at 270 K and 290 K show a metamagnetic behavior with a large hysteresis with the magnetic field inducing reverse transformation from non-magnetic martensite to the ferromagnetic parent phase [39,40]. These results are in accordance with the thermo-magnetization behavior shown in Figure 13.

4 MAGNETIC MATERIALS

4.1 Co-Cr-based Magnetic Recording Media

Co-Cr-based sputtered thin films have a high coercivity (H_c) with a high magnetization (M) and have been widely used as magnetic recording media of hard disks [41]. The thin films have a hexagonal close-packed (hcp) structure and a fine microstructure with the cobalt-rich ferromagnetic phase precipitated in the chromium-rich paramagnetic matrix [42]. The distribution of chromium in each phase and the microstructure have a significant effect on the recording properties of this alloy. Ishida and Nishizawa [43] have suggested that a likely origin of the chromium segregation in a Co-Cr alloy thin film is the miscibility gap in the hcp phase because the thermodynamic calculations of Co-Cr binary system by Hasebe et al. [44] indicate a magnetically

induced miscibility gap in fcc and hcp phases along the Curie temperature. This suggestion is now generally accepted by other researchers. Recently, Oikawa et al. [45] confirmed the miscibility gap along the Curie temperature in several cobalt-base fcc alloys by the diffusion couple technique and reevaluated the thermodynamic properties. The phase diagram in the cobalt-rich portion of the Co-Cr system is shown in Figure 15.

The calculated metastable magnetically induced phase separation in the hcp phase agrees well with the experimental results, strongly implying that the magnetically induced phase separation is responsible for the compositional heterogeneity in Co-Cr-based films.

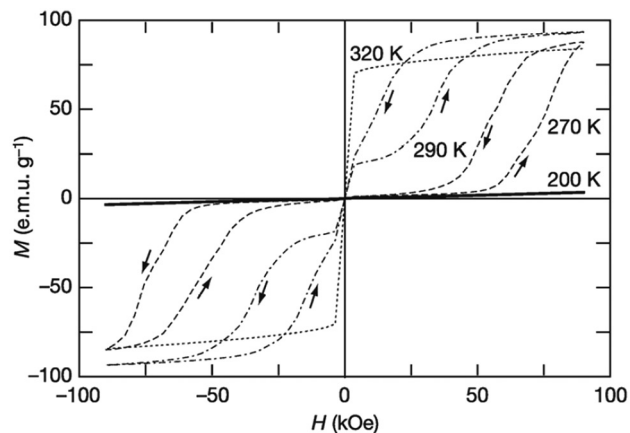


Figure 14. Magnetization versus magnetic field curves for the $Ni_{45}Co_5Mn_{36}In_{13.4}$ alloy between 200K and 320K.

From the thermodynamic calculation of the Co-Cr-X ternary system, the shape of the magnetically induced phase separation in the cobalt-rich portion can be classified into four types as shown in Figure 16 [46].

In Type I, the chromium contents in both the ferromagnetic and paramagnetic phases decrease with an increasing amount of X. In Type II, the chromium content decreases in the ferromagnetic phase and increases in the paramagnetic phase with an increasing amount of X. In Type III, the chromium content of the paramagnetic phase is increased by the addition of X, whereas that in the ferromagnetic phase is not effectively reduced. Finally, in Type IV, the three-phase equilibrium of one ferromagnetic and two paramagnetic phases is formed. Figure 17 shows the classification of the effect of the alloying elements on the phase equilibria of the Co-Cr system in the periodic table based on the calculated results.

Pd, Rh and Ir show a type of miscibility gap similar to that of the Co-Cr-Pt phase diagram. The magnetic properties of the Co-Cr-Pd thin-film alloy would be expected to be similar to those of the Co-Cr-Pt system. On the other hand, the addition of iridium to cobalt strongly decreases the magnetic anisotropy energy (MAE), which in turn would cancel out the beneficial effect of decreasing chromium content in the ferromagnetic phase by the alloying of iridium [47]. This means that the MAE of each binary system, as well as the phase diagram, should be considered for the material design of Co-Cr-based high-density magnetic recording media.

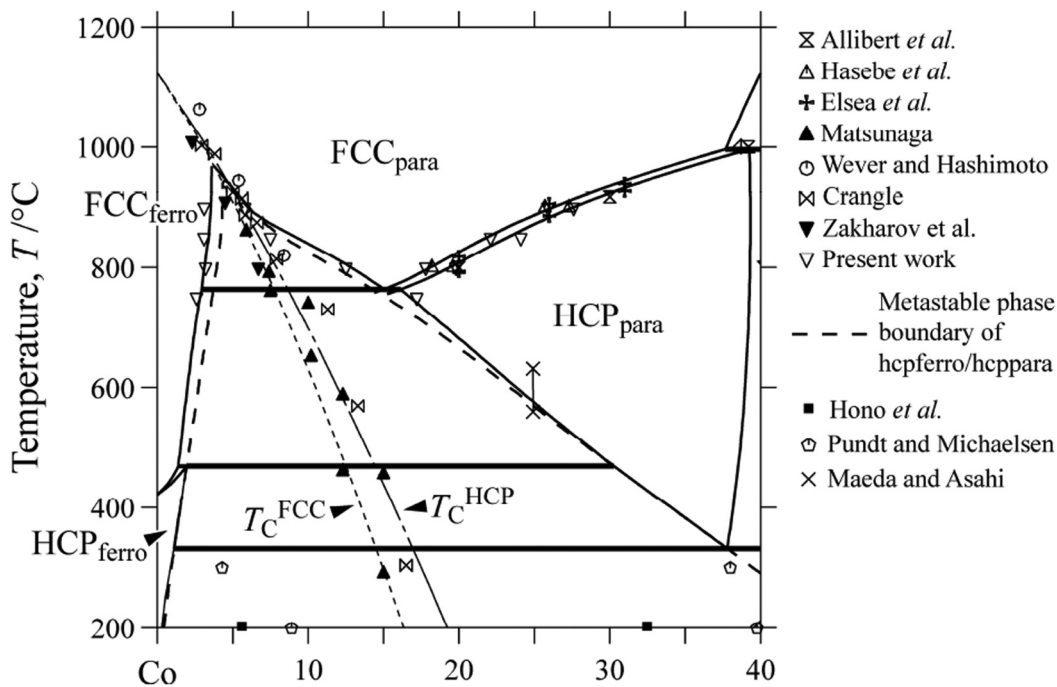


Figure 15. Phase diagram of the Co-Cr system in the Co-rich portion from Oikawa et al. [45]. See Oikawa et al. [45] for further information.

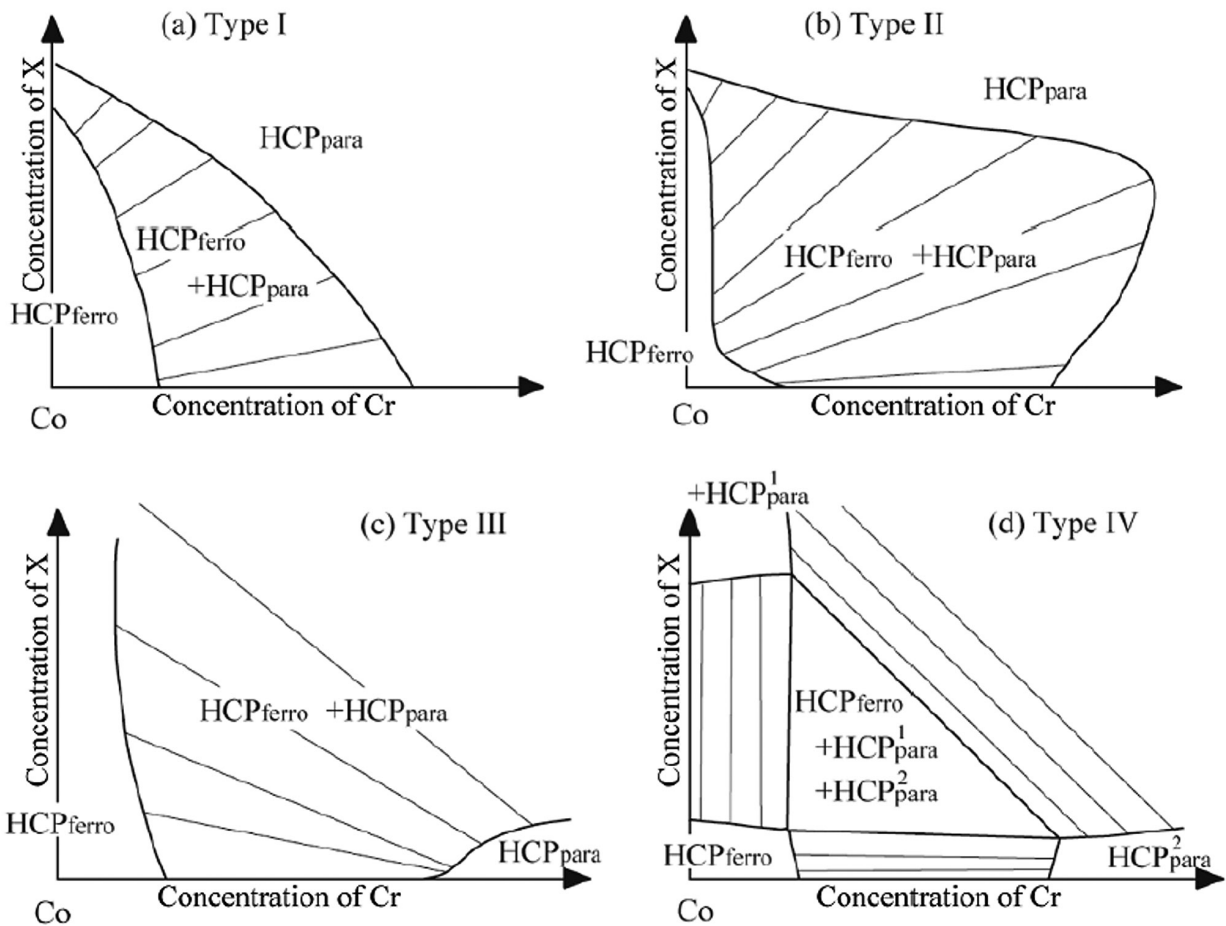


Figure 16. Types of two-phase separation of hcp phase in the Co-Cr-X ternary systems. (a) Type I; (b) Type II; (c) Type III and (d) Type IV.

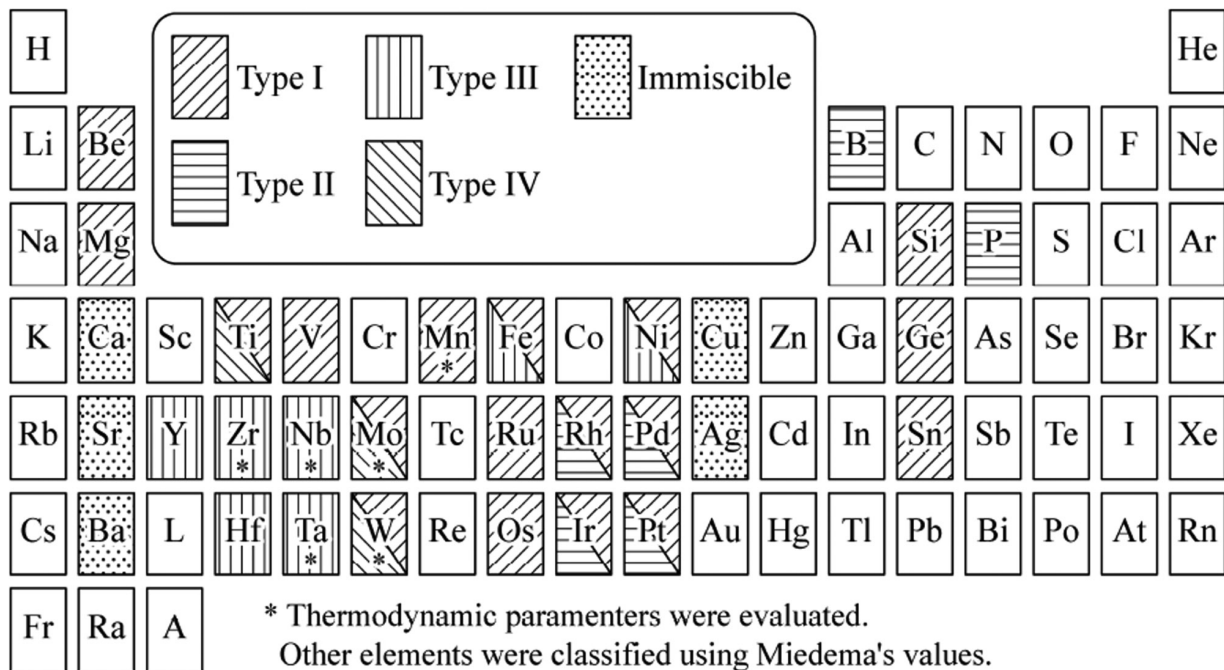


Figure 17. Classification of elements in the Periodic Table for the miscibility gap of the hcp phase in the Co-Cr-X system.

4.2 Ferromagnetic Heusler Alloys

Since the ferromagnetic Cu_2MnAl phase was discovered by Fritz Heusler in 1903, more than 1000 compounds have become known as Heusler compounds [48]. These compounds are very attractive for use as multi-functional materials in magnetic recording, superconductors, shape memory, thermoelectrics, etc. The phase stability of Heusler compounds is the basic information for the development of functional materials. The present authors' group has investigated the phase stability of Co-based and Ni-based Heusler compounds. Figure 18 shows the ordering and phase separation between the $B2$ and $L2_1$ (Heusler) phases in the $X_2\text{AlTi}$ ($X=\text{Fe}, \text{Co}, \text{Ni}, \text{Cu}$) compounds [49].

Surprisingly, the phase stability, i.e., the maximum temperature of the $B2/L2_1$ ordering (${}^{\text{max}}T_C^{B2/L2_1}$), the tricritical temperature ($T_t^{B2/L2_1}$) and the phase boundaries of miscibility gap between $B2$ and $L2_1$ phases, can be predicted by the valence electron concentration of the X site atoms. Figure 19 shows the relation between the critical temperatures and $3d + 4s$ electron concentration in the X site. Figure 20 shows the $T_C^{B2/L2_1}$ and Curie temperature T_C as a function of a number of valence electron of $3d$ in the Y elements in Co_2YZ

($Y=\text{Ti}, \text{V}, \text{Cr}, \text{Mn}, \text{Fe}$ and $Z=\text{Al}, \text{Ga}$) Heusler alloys [49-51]. T_C increases with the increase of N_{3d} and the values are not so different between the Al and Ga series. On the other hand, $T_t^{B2/L2_1}$ tends to indicate behavior opposite to that of T_C , i.e., $T_t^{B2/L2_1}$ decreases with the increase of N_{3d} except for $Y = \text{Cr}$. Although the tendency of $T_t^{B2/L2_1}$ as a function of N_{3d} is similar with respect to one another, $Z = \text{Al}$ and Ga , actual values of $T_t^{B2/L2_1}$ for $Z = \text{Ga}$ are higher than that of the $Z = \text{Al}$ series in whole. The Co-based Heusler alloys with higher values of $T_t^{B2/L2_1}$ are easier to order to the $L2_1$ -type structure. This means that the confirmation of $T_t^{B2/L2_1}$ is very valuable to efficiently heighten the degree of order by thermal annealing in industrial processing and is a very important component in the technology of spintronics [52].

5 HIGH TEMPERATURE MATERIALS

5.1 Ni-base Superalloys

Ni-base superalloys are widely used as high-temperature materials in aircraft engines, gas turbines, reactors, chemical industry, etc., where the γ' phase of Ni_3Al with the $L1_2$

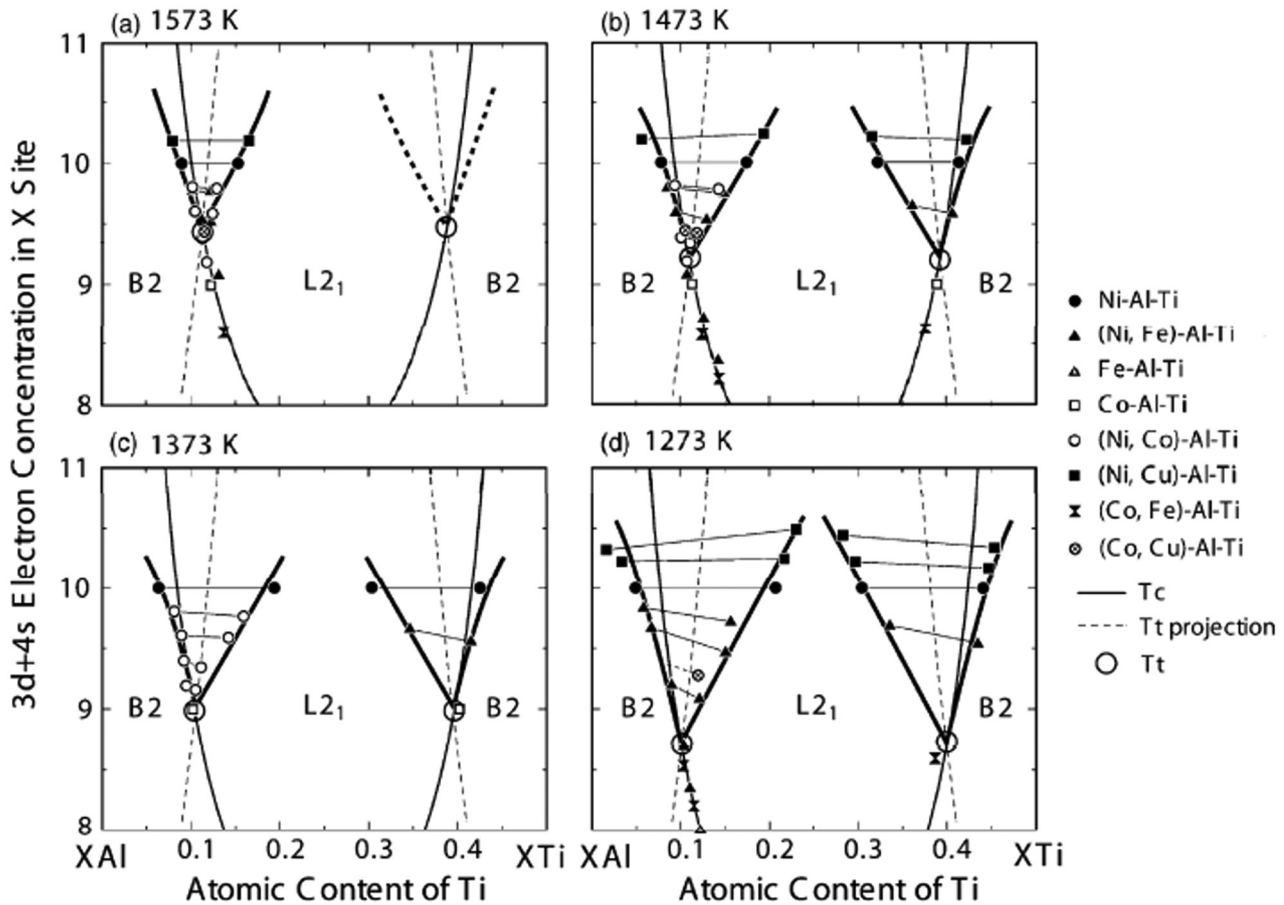


Figure 18. Composition of the calculated and experimentally obtained phase equilibria between the $B2$ and $L2_1$ phases at (a) 1573K; (b) 1473K; (c) 1373K and (d) 1273K.

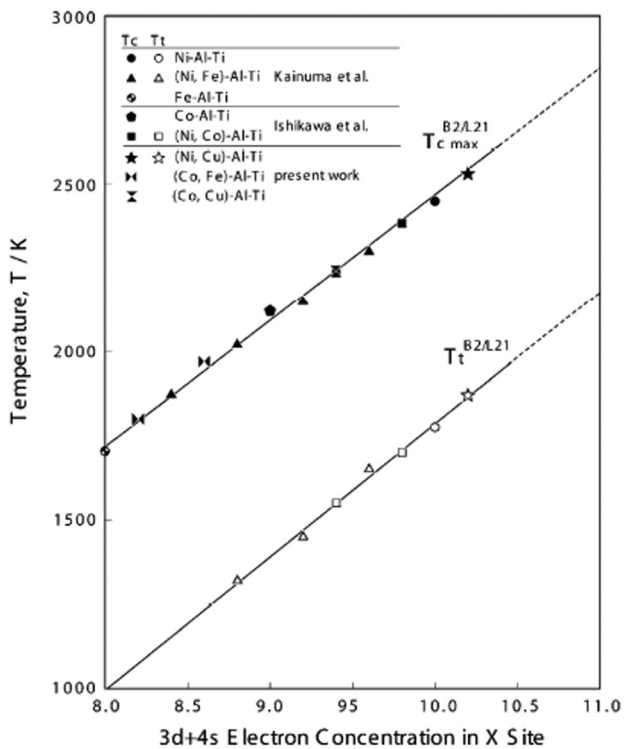


Figure 19. The critical temperatures of $T_c^{B2/L21}$ and $T_t^{B2/L21}$ evaluated by extrapolation from the experimental data vs $3d+4s$ electron number of Fe, Co, Ni and Cu. See Ishikawa et al. [49] for details.

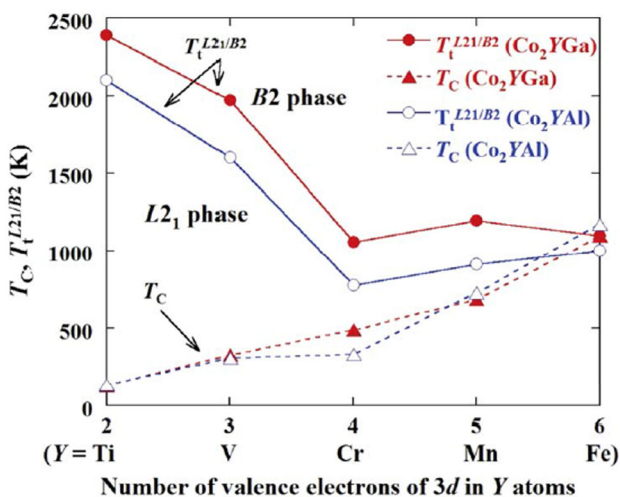


Figure 20. Order-disorder phase transition temperatures from $L2_1$ to B2 phase, $T_t^{B2/L21}$ and Curie temperature, T_c , as a function of the number of valence electrons for $3d$ in Y elements for Co_2YZ ($Y=Ti, V, Cr, Mn, Fe$ and $Z=Al, Ga$) alloys.

structure plays a key role in maintaining strength at higher temperatures [53], while the strengthening mechanism utilized Co-base high temperature alloys is principally due to the solid solution hardening with refractory element and carbide precipitation [54]. This difference in the strengthening phase of Ni-base and Co-base alloy is due to the existence of the γ' phase as shown in Figure 21, where the stable γ'

phase of Ni_3Al appears at up to $1395^\circ C$, while no Co_3Al compound is formed.

The β ($NiAl, CoAl$; B2) phase has been used for the surface coating of Ni-base superalloys because of its high resistance to oxidation [55]. Therefore, data on phase equilibria involving the γ (A1), γ' ($L1_2$) and β (B2) phases in the Ni-Al-base system are fundamentally important for the practical design of Ni-base superalloys. Figure 22 shows the isothermal phase diagrams relating to the γ , γ' and β phases in the Ni-Al-X ternary systems [56], where the phase relations can be classified into six categories depending on the tie line and the existence of the γ' phase. The upper part of the diagrams in Figure 22 shows that the γ' phase disappears with alloying elements such as Mn, Cr, Fe, Co and Cu, while lower part of the diagrams shows that Ti, V, Ta, Mo, W and Si stabilize the γ' phase and that no direct γ/β equilibrium is obtained.

The partition behavior of alloying elements among the γ , γ' and β phases is shown in Figure 23.

The tendency for partitioning among the γ , γ' and β phases is strongly related to the stability of Ni_3X , NiX , and XAl compounds in the binary systems. For example, the elements X forming stable Ni_3X , such as Ti, Zr, Hf, V, Nb, Ta, Si, Ge, and Sn, are strong γ' formers. Such a concept about the expected tendency of alloying elements in stabilizing the γ , γ' and β phases is very useful in designing and improving the ductility of γ' (Ni_3Al) and β ($NiAl$) base alloys.

5.2 Co-base Superalloys

Although no γ' Co_3Al compound is formed in the Co-Al binary system as shown in Figure 21, from the viewpoint of enthalpy of formation of Ni_3Al and Co_3Al estimated by Miedema et al. [57], the difference in ΔH for both compounds is small [58], which suggests that a metastable compound with the $L1_2$ structure of the Co_3X would be expected to appear. In fact, the metastable γ' phase of Co_3Al [59] and of Co_3Ta [60] is confirmed. In 2006, the authors' group found the γ' phase of $Co_3(Al,W)$ with the $L1_2$ structure [61]. The SEM micrographs of this $\gamma + \gamma'$ structure of Co-base ternaries are shown in Figure 24, where the cuboidal γ' phase homogeneously precipitates in the γ (A1) matrix, which is very similar to the morphology of conventional Ni-base superalloys [61].

The phase diagram of the Co-Al-W ternary system at $900^\circ C$ is shown in Figure 25, and the composition of cuboidal precipitates observed in Figure 24 is the ternary compound of $Co_3(Al,W)$, where the composition of Al and W has an almost equiatomic ratio. Although the γ' phase at $900^\circ C$ in Figure 25 is metastable [62], the γ' phase is stabilized by alloying, Ni [63], Ta, Ti, etc. Figure 26 shows the effect of alloying elements on the partitioning behavior between the γ and γ' phases in Co-8.8Al-9.8W-2X (at.%) alloys [64] as a function of temperature, which is compared with that of the Ni-Al-X ternary systems [56].

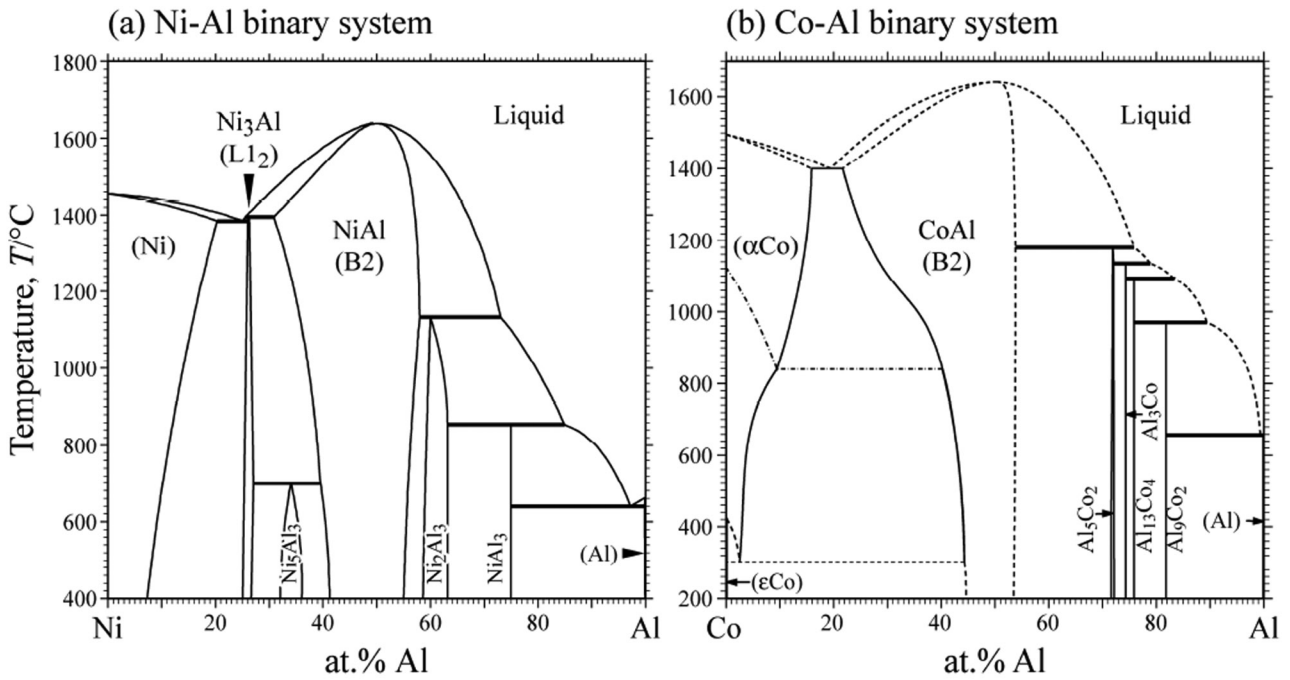


Figure 21. Phase diagrams of the (a) Ni-Al and (b) Co-Al systems.

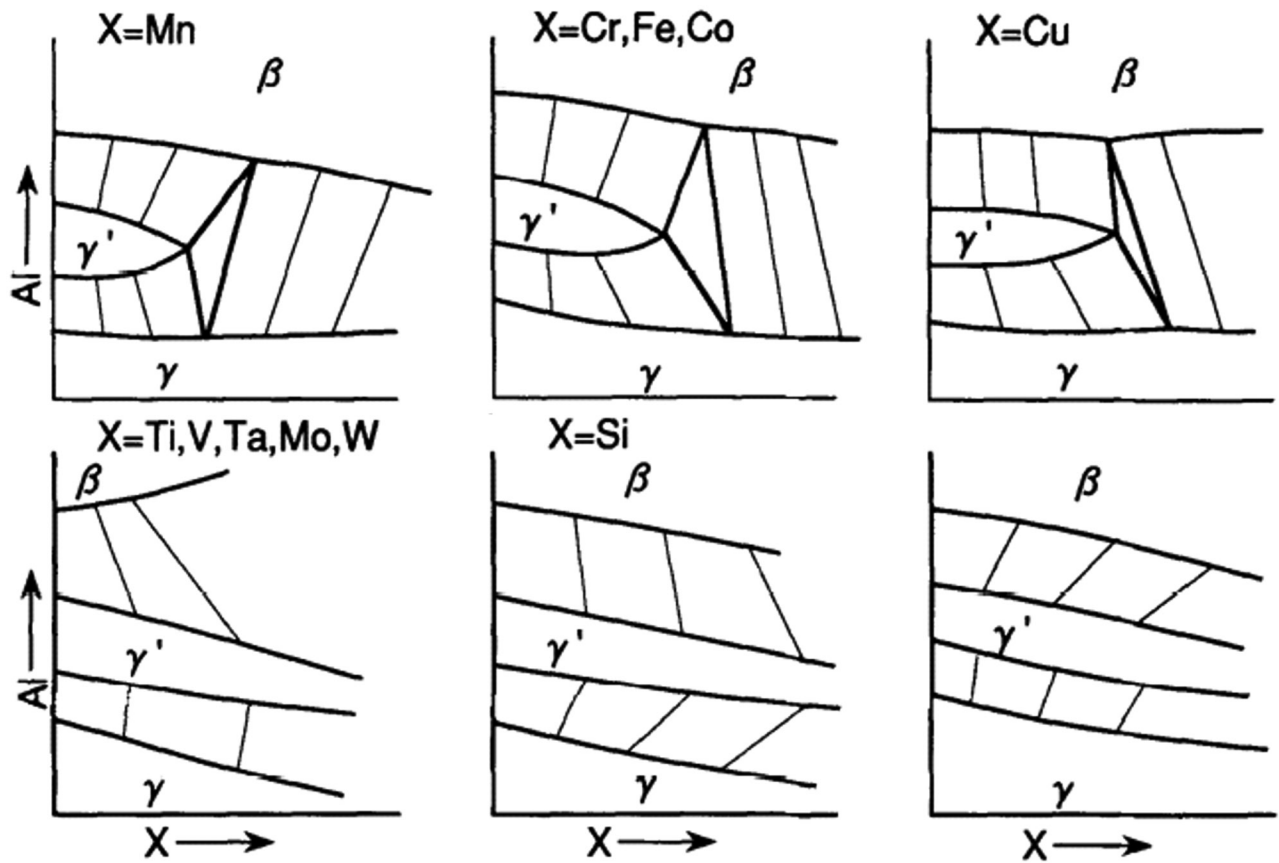


Figure 22. Classification of $\gamma/\gamma'/\beta$ phase equilibria in the Ni-Al-X ternary systems.

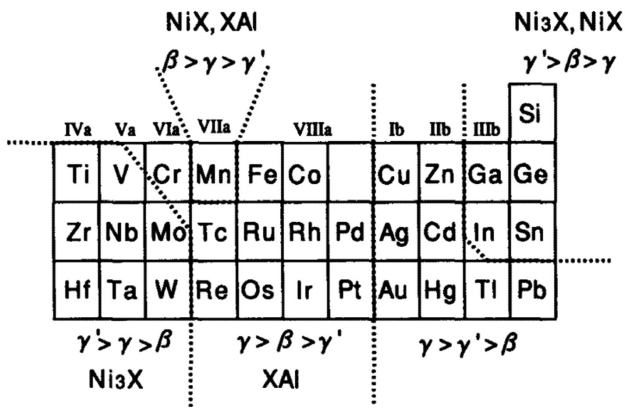


Figure 23. Effect of alloying elements on the relative stability of the γ , γ' (Ni_3Al) and β (NiAl) phases.

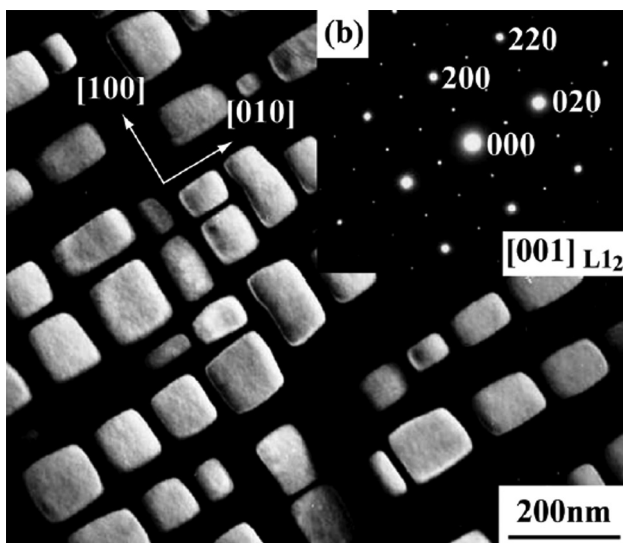


Figure 24. TEM image of Co-9Al-7.5W (at.%) alloy heat-treated at 900°C for 72 hours.

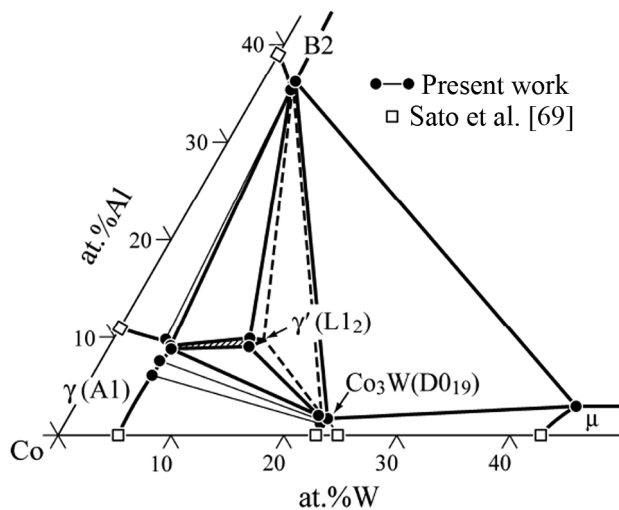


Figure 25. Isothermal section phase diagrams of the Co-Al-W ternary system in the Co-rich portion at 1173K.

The partitioning behavior of alloying elements in the Co-Al-W-X system is very similar to that of the Ni-Al-X system, where Ta, Nb and Ti are strong γ' stabilizing elements, while Cr, Mn and Fe are γ -forming elements.

High temperature strength and deformation of the $\gamma + \gamma'$ two-phase structure of Co-Al-W base alloys have been studied [65-67], results showing that the positive temperature dependence of flow stress is observed above 600°C in Co-Al-W-base alloys similar to that of Ni-base superalloys. The creep properties of Co-Al-W-base alloys have been reported [68], the strength of these alloys being comparable to that of the Ni-base superalloys of the first generation.

Cast Co-base superalloys have been developed for application in friction stir welding (FSW) tools [69]. FSW is a solid state joining technology that can be used to weld most Al alloys, where the tool steel is used as a joining tool. However, FSW tools that enable welding of high-softening-temperature materials such as steels and titanium alloys are very limited. W-Re and polycrystalline cubic boron nitride (PCBN) tools have been developed, but they are too expensive to be used. Cast Co-Ni-Al-W-base alloys have been applied as a new tool material, which enables FSW for Ti-base alloys, mild steel, Cu- and Zr-base alloys [69]. The Co-base tools for FSW are produced by a lost-wax process and then heat-treated to obtain the γ' phase in the matrix. The weld appearance of Ti-6Al-4V is shown in Figure 27, where a new Co-base alloy tool produces a defect-free weld with a smooth, shiny surface.

Although, development of Co-base superalloys using the γ' $\text{Co}_3(\text{Al,W})$ phase has just been started, significant results have already been obtained. This is because phase equilibria, alloying behavior, microstructural control, mechanical properties, etc., of Co-base superalloys are very

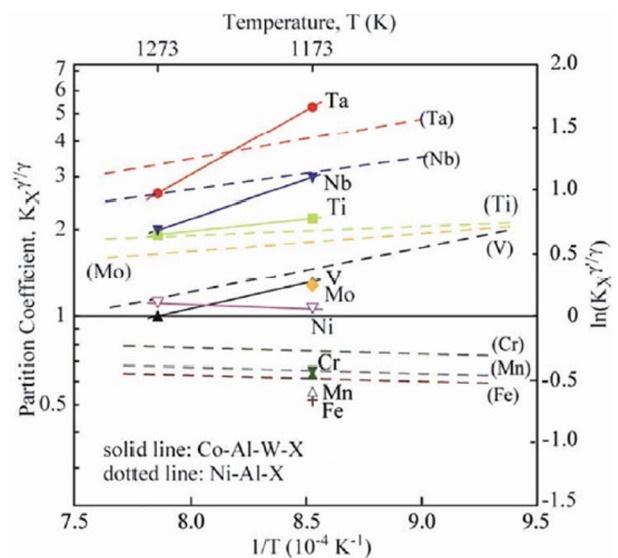


Figure 26. Effect of alloying elements on distribution coefficient between the γ and γ' phases in the Co-Al-W-X systems.

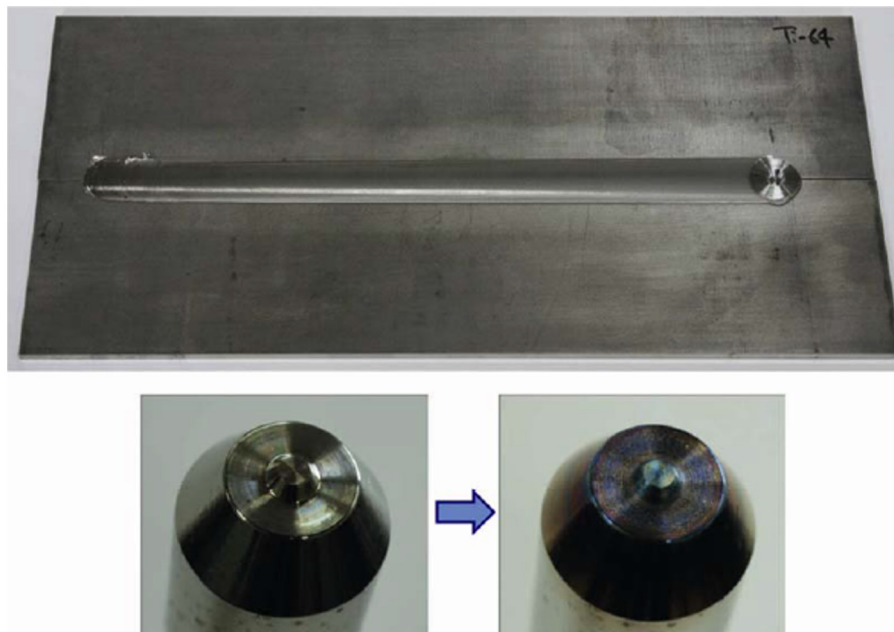


Figure 27. FSW appearance of Ti-6Al-4V alloy using a Co-base alloy tool.

similar to that of Ni-base superalloys. There is no doubt that the Co-base superalloys using the γ' $\text{Co}_3(\text{Al,W})$ phase have great potential for a new class of high-temperature, high-strength structural materials.

Cu-base alloys. In addition, examples for development of shape memory alloys, Co-Cr base magnetic recording media and high-temperature alloys using the γ' phase with the aid of phase diagrams were also introduced.

6. SUMMARY

A thermodynamic tool for design of materials in electronic packaging has been developed on the basis of the CALPHAD method. This tool can provide much valuable information on thermodynamics such as stable and metastable phase equilibria, phase fraction, etc. Examples were herein given to demonstrate the great utility of these databases for designing Pb-free solders and high-strength

Acknowledgements

The authors would like to thank Profs. R. Kainuma, K. Oikawa, Y. Sutou, T. Omori, Y. Sato, R.Y. Umetsu and Y. Araki for their help. This work was supported by a Grant-in-Aid for Science Research from the Japan Society for the Promotion of the Science. One of the authors (K.I.) acknowledges the support from Toyota Physical & Chemical Research Institute.

REFERENCES

- 1 Kaufman L, Bernstein H. Computer calculation of phase diagrams. New York: Academic Press; 1970.
- 2 Nishizawa T. Progress of CALPHAD. Materials Transactions. 1992;33(8):713-722. <http://dx.doi.org/10.2320/matertrans1989.33.713>.
- 3 Saunders N, Miodownik AP. CALPHAD. Lausanne: Pergamon; 1998.
- 4 Sundman B, Jansson B, Andersson J-O. The Thermo-Calc databank system. Calphad. 1985;9(2):153-190. [http://dx.doi.org/10.1016/0364-5916\(85\)90021-5](http://dx.doi.org/10.1016/0364-5916(85)90021-5).
- 5 Eriksson G, Hack K. Calculation of phase equilibria in multicomponent alloy systems using a specially adapted version of the program 'SOLGASMIX'. Calphad. 1984;8(1):15-24. [http://dx.doi.org/10.1016/0364-5916\(84\)90025-7](http://dx.doi.org/10.1016/0364-5916(84)90025-7).
- 6 Bale CW, Chartrand P, Degterov SA, Eriksson G, Hack K, Ben Mahfoud R, et al. FactSage thermochemical software and databases. Calphad. 2002;26(2):189-228. [http://dx.doi.org/10.1016/S0364-5916\(02\)00035-4](http://dx.doi.org/10.1016/S0364-5916(02)00035-4).
- 7 Chen SL, Daniel S, Zhang F, Chang YA, Oates WA, Schmid-Fetzer R. On the calculation of multicomponent stable phase diagrams. Journal of Phase Equilibria. 2001;22(4):373-378. <http://dx.doi.org/10.1361/105497101770332910>.

- 8 Ohnuma I, Liu XJ, Ohtani H, Ishida K. Thermodynamic database for phase diagrams in micro-soldering alloys. *Journal of Electronic Materials*. 1999;28(11):1163. <http://dx.doi.org/10.1007/s11664-999-0152-5>.
- 9 Ohnuma I, Liu XJ, Ohtani H, Ishida K. In: Thermodynamic database for micro-soldering alloys. Grassie K, Tenckhoff E, Wegner G, Haubell J, Hanselka H, editors. Weinheim: Wiley-VCH; 2000. 69 p.
- 10 Ohnuma I, Liu XJ, Kainuma R, Ohtani H, Chen SL, Chang YA, Ishida K. Development of thermodynamic tool "ADAMIS/Pandat" and its application in design of micro-soldering materials. In: Proceedings of Annual Congress of ABM; 2003. p. 897-903.
- 11 Liu XJ, Ohnuma I, Wang CP, Jiang M, Kainuma R, Ishida K, et al. Thermodynamic database on microsolders and copper-based alloy systems. *Journal of Electronic Materials*. 2003;32(11):1265-1272. <http://dx.doi.org/10.1007/s11664-003-0021-6>.
- 12 Wang CP, Liu XJ, Jiang M, Ohnuma I, Kainuma R, Ishida K. Thermodynamic database of the phase diagrams in copper base alloy systems. *Journal of Physics and Chemistry of Solids*. 2005;66(2-4):256-260. <http://dx.doi.org/10.1016/j.jpcs.2004.08.037>.
- 13 Vianco PT, Frear DR. Issues in the replacement of lead-bearing solders. *Journal of The Minerals, Metals & Materials Society*. 1993;45(7):14-19. <http://dx.doi.org/10.1007/BF03222374>.
- 14 Liu XJ, Oikawa K, Ohnuma I, Kainuma R, Ishida K. The use of phase diagrams and thermodynamic databases for electronic materials. *JOM*. 2003;55(12):53-59. <http://dx.doi.org/10.1007/s11837-003-0012-3>.
- 15 Wang CP, Liu XJ, Ohnuma I, Kainuma R, Ishida K. Formation of immiscible alloy powders with egg-type microstructure. *Science*. 2002;297(5583):990-993. <http://dx.doi.org/10.1126/science.1073050>. PMID:12169728.
- 16 Zhao JZ, He J, Hu ZQ, Ratke L. Microstructure evolution in immiscible alloys during rapid directional solidification. *Zeitschrift fur Metallkunde*. 2004;95(5):362-368. <http://dx.doi.org/10.3139/146.017967>.
- 17 Wu M, Ludwig A, Pelzer M, Postl U. On the Impact of Macroscopic Phase Separation on Solidification Microstructures. *Advanced Engineering Materials*. 2005;7(9):846-851. <http://dx.doi.org/10.1002/adem.200500098>.
- 18 He J, Zhao JZ, Ratke L. Solidification microstructure and dynamics of metastable phase transformation in undercooled liquid Cu-Fe alloys. *Acta Materialia*. 2006;54(7):1749-1757. <http://dx.doi.org/10.1016/j.actamat.2005.12.023>.
- 19 Kaptay G. Classification and general derivation of interfacial forces, acting on phases, situated in the bulk, or at the interface of other phases. *Journal of Materials Science*. 2005;40:2125.
- 20 Wang CP, Liu XJ, Kainuma R, Takaku Y, Ohnuma I, Ishida K. Formation of core-type macroscopic morphologies in Cu-Fe base alloys with liquid miscibility gap. *Metallurgical and Materials Transactions. A, Physical Metallurgy and Materials Science*. 2004;35(4):1243-1253. <http://dx.doi.org/10.1007/s11661-004-0298-y>.
- 21 Takaku Y, Ohnuma I, Kainuma R, Yamada Y, Yagi Y, Nishibe Y, et al. Development of Bi-base high-temperature Pb-free solders with second-phase dispersion: thermodynamic calculation, microstructure, and interfacial reaction. *Journal of Electronic Materials*. 2006;35(11):1926-1932. <http://dx.doi.org/10.1007/s11664-006-0295-6>.
- 22 Yamada Y, Takaku Y, Yagi Y, Nakagawa I, Atsumi T, Shirai M, et al. Pb-free high temperature solders for power device packaging. *Microelectronics and Reliability*. 2006;46(9-11):1932-1937. <http://dx.doi.org/10.1016/j.microrel.2006.07.083>.
- 23 Yamada Y, Takaku Y, Yagi Y, Nakagawa I, Atsumi T, Shirai M, et al. Reliability of wire-bonding and solder joint for high temperature operation of power semiconductor device. *Microelectronics and Reliability*. 2007;47(12):2147-2151. <http://dx.doi.org/10.1016/j.microrel.2007.07.102>.
- 24 Ohnuma I, Saegusa T, Takaku Y, Wang CP, Liu XJ, Kainuma R, et al. Microstructural Evolution of Alloy Powder for Electronic Materials with Liquid Miscibility Gap. *Journal of Electronic Materials*. 2009;38(1):2-9. <http://dx.doi.org/10.1007/s11664-008-0537-x>.
- 25 Miyamoto T, Nagasako M, Kainuma R. Phase equilibria in the Ni-Mn-In alloy system. *Journal of Alloys and Compounds*. 2013;549:57-63. <http://dx.doi.org/10.1016/j.jallcom.2012.08.128>.
- 26 Tadaki T. Cu-based shape memory alloys. In: Otsuka K, Wayman CM, editors. Shape memory materials. Cambridge: Cambridge University Press; 1998. p. 97.
- 27 Kainuma R, Takahashi S, Ishida K. Thermoelastic martensite and shape memory effect in ductile Cu-Al-Mn alloys. *Metallurgical and Materials Transactions. A, Physical Metallurgy and Materials Science*. 1996;27(8):2187-2195. <http://dx.doi.org/10.1007/BF02651873>.
- 28 Koster W, Godecke T. Das Dreistoffsystem Kupfer-Mangan-Aluminium. *Zeitschrift fur Metallkunde*. 1966;57:889.

- 29 Kainuma R, Satoh N, Liu XJ, Ohnuma I, Ishida K. Phase equilibria and Heusler phase stability in the Cu-rich portion of the Cu–Al–Mn system. *Journal of Alloys and Compounds*. 1998;266(1-2):191-200. [http://dx.doi.org/10.1016/S0925-8388\(97\)00425-8](http://dx.doi.org/10.1016/S0925-8388(97)00425-8).
- 30 Sutou Y, Omori T, Kainuma R, Ishida K, Yamauchi K. Development of Cu-Al-Mn-based shape memory alloys with enhanced ductility. *Materia*. 2003;42(11):813-821. <http://dx.doi.org/10.2320/materia.42.813>.
- 31 Sutou Y, Omori T, Yamauchi Y, Ono N, Kainuma R, Ishida K. Effect of grain size and texture on pseudoelasticity in Cu–Al–Mn-based shape memory wire. *Acta Materialia*. 2005;53(15):4121-4133. <http://dx.doi.org/10.1016/j.actamat.2005.05.013>.
- 32 Omori T, Kusama T, Kawata S, Ohnuma I, Sutou Y, Araki Y, et al. Abnormal grain growth induced by cyclic heat treatment. *Science*. 2013;341(6153):1500-1502. <http://dx.doi.org/10.1126/science.1238017>. PMID:24072918.
- 33 Ishibashi M, Tabata N, Suetake T, Omori T, Sutou Y, Kainuma R, et al. A simple method to treat an ingrowing toenail with a shape-memory alloy device. *The Journal of Dermatological Treatment*. 2008;19(5):291-292. <http://dx.doi.org/10.1080/09546630701759595>. PMID:19160535.
- 34 Araki Y, Endo T, Omori T, Sutou Y, Koetaka Y, Kainuma R, et al. Potential of superelastic Cu-Al-Mn alloy bars for seismic applications. *Earthquake Engineering & Structural Dynamics*. 2011;40(1):107-115. <http://dx.doi.org/10.1002/eqe.1029>.
- 35 Ullakko K, Huang JK, Kantner C, O'Handley RC, Kokorin VV. Large magnetic-field-induced strains in Ni₂MnGa single crystals. *Applied Physics Letters*. 1996;69(13):1966. <http://dx.doi.org/10.1063/1.117637>.
- 36 James RD, Wuttig M. Magnetostriction of martensite. *Philosophical Magazine A*. 1998;77(5):1273-1299. <http://dx.doi.org/10.1080/01418619808214252>.
- 37 O'Handley RC. Model for strain and magnetization in magnetic shape-memory alloys. *Journal of Applied Physics*. 1998;83(6):3263. <http://dx.doi.org/10.1063/1.367094>.
- 38 Sutou Y, Imano Y, Koeda N, Omori T, Kainuma R, Ishida K, et al. Magnetic and martensitic transformations of NiMnX(X=In,Sn,Sb) ferromagnetic shape memory alloys. *Applied Physics Letters*. 2004;85(19):4358-4360. <http://dx.doi.org/10.1063/1.1808879>.
- 39 Kainuma R, Imano Y, Ito W, Sutou Y, Morito H, Okamoto S, et al. Magnetic-field-induced shape recovery by reverse phase transformation. *Nature*. 2006;439(7079):957-960. <http://dx.doi.org/10.1038/nature04493>. PMID:16495995.
- 40 Kainuma R, Oikawa K, Ito W, Sutou Y, Kanomata T, Ishida K. Metamagnetic shape memory effect in NiMn-based Heusler-type alloys. *Journal of Materials Chemistry*. 2008;18(16):1837. <http://dx.doi.org/10.1039/b713947k>.
- 41 Weller D, Doerner MF. *Annual Review of Materials Science*. 2000;30:661.
- 42 Hono K, Babu SS, Maeda Y, Hasegawa N, Sakurai T. Atom probe compositional analysis of Co-Cr sputtered magnetic thin films. *Applied Physics Letters*. 1993;62(20):2504. <http://dx.doi.org/10.1063/1.109336>.
- 43 Ishida K, Nishizawa T. Role of Miscibility Gap in Magnetic Alloys: Alnico, Fe-Cr-Co and Co-Cr. In: Hayes FH, editor. *Proceedings of International Conference. on User Aspects of Phase Diagrams*; 1991. London: Institute of Metals; 1991. 185 p.
- 44 Hasebe M, Oikawa K, Nishizawa T. Computer Calculation of Phase Diagrams of Co-Cr and Co-Mn Systems. *Journal of the Japan Institute of Metals and Materials*. 1982;46:577.
- 45 Oikawa K, Qin GW, Ikeshoji T, Kainuma R, Ishida K. Direct evidence of magnetically induced phase separation in the fcc phase and thermodynamic calculations of phase equilibria of the Co–Cr system. *Acta Materialia*. 2002;50(9):2223-2232. [http://dx.doi.org/10.1016/S1359-6454\(01\)00433-5](http://dx.doi.org/10.1016/S1359-6454(01)00433-5).
- 46 Oikawa K, Qin GW, Kitakami O, Shimada Y, Fukamichi K, Ishida K. Prediction of effective elements for magnetically induced phase separation in Co–Cr-based magnetic recording media. *Applied Physics Letters*. 2001;79(5):644. <http://dx.doi.org/10.1063/1.1389067>.
- 47 Kikuchi N, Kitakami O, Okamoto S, Shimada Y, Sakuma A, Otani Y, et al. Influence of 5d transition elements on the magnetocrystalline anisotropy of hcp-Co. *J. Phys. Cond. Mat.* 1999;11(43):L485-L490. <http://dx.doi.org/10.1088/0953-8984/11/43/103>.
- 48 Graf T, Felser C, Parkin SSP. Simple rules for the understanding of Heusler compounds. *Progress in Solid State Chemistry*. 2011;39(1):1-50. <http://dx.doi.org/10.1016/j.progsolidstchem.2011.02.001>.
- 49 Ishikawa K, Kainuma R, Ohnuma I, Aoki K, Ishida K. Phase stability of the X₂AlTi (X: Fe, Co, Ni and Cu) Heusler and B2-type intermetallic compounds. *Acta Materialia*. 2002;50(9):2233-2243. [http://dx.doi.org/10.1016/S1359-6454\(01\)00434-7](http://dx.doi.org/10.1016/S1359-6454(01)00434-7).

- 50 Kobayashi K, Umetsu RY, Fujita A, Oikawa K, Kainuma R, Fukamichi K, et al. Magnetic properties and phase stability of half-metal-type $\text{Co}_2\text{Cr}_{1-x}\text{Fe}_x\text{Ga}$ alloys. *Journal of Alloys and Compounds*. 2005;399(1-2):60-63. <http://dx.doi.org/10.1016/j.jallcom.2005.03.037>.
- 51 Kobayashi K, Ishikawa K, Umetsu RY, Kainuma R, Aoki K, Ishida K. Phase stability of B2 and L2_1 ordered phases in Co_2YGa (Y=Ti, V, Cr, Mn, Fe) alloys. *Journal of Magnetism and Magnetic Materials*. 2007;310(2):1794-1795. <http://dx.doi.org/10.1016/j.jmmm.2006.10.704>.
- 52 Umetsu RY, Okubo A, Nagasako M, Ohtsuka M, Kainuma R, Ishida K. Phase stability of L2_1 phase in Co-based heusler alloys. *Spin*. 2014;4(04):1440018. <http://dx.doi.org/10.1142/S2010324714400189>.
- 53 Ross EW, Sims CT. *Superalloys II*. New York: John Wiley & Sons; 1987. 97 p.
- 54 Beltran AM. *Superalloys II*. New York: John Wiley & Sons; 1987. 135 p.
- 55 Wood TE, Goldman E. *Superalloys II*. New York: John Wiley & Sons; 1987. 359 p.
- 56 Jia CC, Ishida K, Nishizawa T. Partition of alloying elements between γ (Al), γ' (L1_2), and β (B2) phases in Ni-Al base systems. *Metallurgical and Materials Transactions. A, Physical Metallurgy and Materials Science*. 1994;25A(3):473-485. <http://dx.doi.org/10.1007/BF02651589>.
- 57 Miedema AR, Boer FR, Boom R, Mattens WCM, Niessen AK. *Cohesion in metals: transition metal alloys*. Amsterdam: North-Holland; 1989.
- 58 Ishida K. Intermetallic compounds in Co-base alloys-phase stability and application to superalloys. *Proceedings of the Materials Research Society*. 2009;1128:357.
- 59 Omori T, Sutou Y, Oikawa K, Kainuma R, Ishida K. Shape memory and magnetic properties of Co-Al ferromagnetic shape memory alloys. *Materials Science and Engineering A*. 2006;438-440:1045-1049. <http://dx.doi.org/10.1016/j.msea.2005.12.068>.
- 60 Shinagawa K, Chinen H, Omori T, Oikawa K, Ohnuma I, Ishida K, et al. Phase equilibria and thermodynamic calculation of the Co-Ta binary system. *Intermetallics*. 2014;49:87-97. <http://dx.doi.org/10.1016/j.intermet.2014.01.015>.
- 61 Sato J, Omori T, Oikawa K, Ohnuma I, Kainuma R, Ishida K. Cobalt-base high-temperature alloys. *Science*. 2006;312(5770):90-91. <http://dx.doi.org/10.1126/science.1121738>. PMID:16601187.
- 62 Kobayashi S, Tsukamoto Y, Takasugi T, Chinen H, Omori T, Ishida K, et al. Determination of phase equilibria in the Co-rich Co-Al-W ternary system with a diffusion-couple technique. *Intermetallics*. 2009;17(12):1085-1089. <http://dx.doi.org/10.1016/j.intermet.2009.05.009>.
- 63 Shinagawa K, Omori T, Sato J, Oikawa K, Ohnuma I, Kainuma R, et al. Phase Equilibria and Microstructure on γ' Phase in Co-Ni-Al-W System. *Materials Transactions*. 2008;49(6):1474-1479. <http://dx.doi.org/10.2320/matertrans.MER2008073>.
- 64 Omori T, Oikawa K, Sato J, Ohnuma I, Kattner UR, Kainuma R, et al. Partition behavior of alloying elements and phase transformation temperatures in Co-Al-W-base quaternary systems. *Intermetallics*. 2013;32:274-283. <http://dx.doi.org/10.1016/j.intermet.2012.07.033>.
- 65 Suzuki A, Pollock TM. High-temperature strength and deformation of γ/γ' two-phase Co-Al-W-base alloys. *Acta Materialia*. 2008;56(6):1288-1297. <http://dx.doi.org/10.1016/j.actamat.2007.11.014>.
- 66 Pollock TM, Dibbern J, Tsunekane M, Zhu J, Suzuki A. New Co-based γ - γ' high-temperature alloys. *JOM*. 2010;62:58. <http://dx.doi.org/10.1007/s11837-010-0013-y>.
- 67 Shinagawa K, Omori T, Oikawa K, Kainuma R, Ishida K. Ductility enhancement by boron addition in Co-Al-W high-temperature alloys. *Scripta Materialia*. 2009;61(6):612-615. <http://dx.doi.org/10.1016/j.scriptamat.2009.05.037>.
- 68 Tanaka K, Ooshima M, Tsuno N, Sato A, Inui H. Creep deformation of single crystals of new Co-Al-W-based alloys with fcc/ L1_2 two-phase microstructures. *Philosophical Magazine*. 2012;92(32):4011-4027. <http://dx.doi.org/10.1080/14786435.2012.700416>.
- 69 Sato YS, Miyake M, Kokawa H, Omori T, Ishida K, Imano S, et al. Friction stir welding and processing VI. *TMS*; 2011.

Received: 29 Jan. 2016

Accepted: 2 Feb. 2016